Vector meson photoproduction - model independent aspects

W. M. Kloet[a] and F. Tabakin[b]

[a]Department of Physics and Astronomy, Rutgers University,
Piscataway, New Jersey, USA

[b]Department of Physics and Astronomy, University of Pittsburgh,
Pittsburgh, Pennsylvania, USA

The rich spin structure of vector meson photoproduction allows for a systematic analysis of the angular and energy dependence of the spin observables in the photon-nucleon c.m. frame. Constraints for spin observables based on positivity of the spin density matrix, are discussed and should be part of any future analysis of experimental data.

1. INTRODUCTION

It is now feasible for photoproduction of vector mesons to have full spin information on all initial and final particles. Apart from experiments with polarized photon beam and polarized nucleon target, the angular distribution of the pseudoscalar mesons resulting from the decay of the unstable vector meson gives information about the spin state of the spin-1 vector meson. Furthermore, experiments can now be performed that also determine the polarization of the recoil nucleon.

This allows in the very near future for an abundance of measured spin observables including spin-spin correlations in reactions like $\gamma + N \rightarrow \rho + N$, or $\gamma + N \rightarrow \phi + N$. These spin observables are fingerprints of the underlying reaction mechanism. They serve to distinguish mechanisms due to baryonic and mesonic resonances, which can occur as doorway states in the photoproduction mechanism. Of particular interest are the missing resonances, which are predicted in qqq models, but so far have not been observed in reactions which were mainly induced from the πN channel. Also of importance are exotic resonances which are mesonic states beyond $q\bar{q}$ states.

2. NATURE OF FINGERPRINT

Photoproduction of vector mesons is described [1] by twelve helicity amplitudes

$$H_i(\theta, E) = {}_{out}\!< \lambda_V \lambda_{N'} | T | \lambda_\gamma \lambda_N >_{in}, \tag{1}$$

for the various helicities of the photon (λ_γ), target nucleon (λ_N), vector meson (λ_V), and recoil nucleon ($\lambda_{N'}$). Their angular dependence is governed by the Wigner rotation functions $d^j_{mn}(\theta)$ since each helicity amplitude has the structure

$$H_i(\theta, E) = \sum_j A_j(E)\, d^j_{(\lambda_V - \lambda_{N'})(\lambda_\gamma - \lambda_N)}(\theta). \tag{2}$$

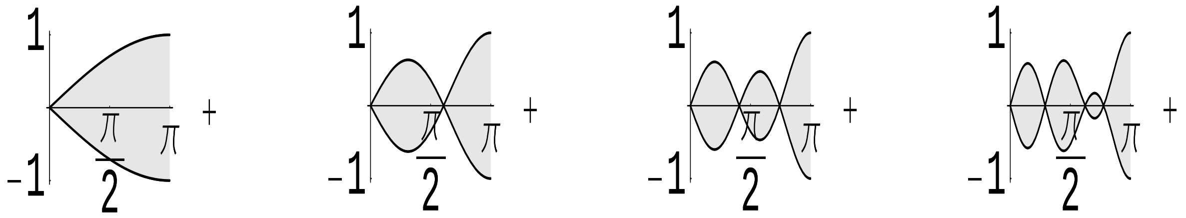

Figure 1. Dependence on production angle θ for $0 \leq \theta \leq \pi$ of leading harmonics in helicity amplitudes corresponding to $m = \lambda_V - \lambda_{N'} = -1/2, n = \lambda_\gamma - \lambda_N = 1/2$.

The cross section $\frac{d\sigma}{d\Omega} \sim \sum_i |H_i|^2$ while the other spin observables fall into three categories. One class of spin observables depends on differences of $|H_i|^2$. A second class of observables represents interferences of the type $\Im(H_i^* H_j)$ while the third class is due to interferences of the type $\Re(H_i^* H_j)$

Because of above Eq. (2) the θ-dependence of each helicity amplitude $H_i(\theta, E)$ is described by a series of harmonics $d^j_{mn}(\theta)$ with an increasing number of nodes. For example if $m = -1/2, n = 1/2$ all harmonics vanish at $\theta = 0$ but are non-zero for $\theta = \pi$, as shown in Fig. 1. This case is similar to the harmonics of a string with one fixed end and one loose end. Other helicity amplitudes behave like [fixed end - fixed end] or [loose end - fixed end] strings respectively.

This is a model independent aspect of the helicity amplitudes and is reflected in the angular dependence of each spin observable.

On the other hand, any model dependence is due to the dynamics, which then determines the intensity of each harmonic. For instance the presence of a resonance in the s-channel of certain angular momentum j will cause the enhancement of corresponding harmonics near the resonance energy. This enhancement should be manifest in the angular and energy behavior of selected spin observables, and could therefore be a clear indication of the role of that specific resonance. Clearly, spin observables represent a wealth of possible information on the dynamics of the process.

3. NEW DATA

New and copious vector meson photoproduction data is expected from JLAB and LEGS. Most likely, these results will be presented in the form of vector meson rest-frame density matrix elements, following earlier procedures [2]. Such a presentation of results is particularly useful for separating exchange mechanisms of natural/unnatural parity particles. However, conventional spin observables, especial double spin observables [3], need to be defined in the photon-nucleon c.m. system. The reason for this is twofold. First, if one deals with spin correlations, there are at least two particles involved and there is no single rest frame. Second, it may be necessary to make use of several relations that exist between the many spin observables, and these relations hold only if all observables refer to the c.m. frame. Thus, one will need to map the above rest-frame results over to the photon-nucleon c.m. system. Subsequently one can investigate the behavior of the various spin observables as a function of production angle and energy as given by Eq. (2), which may reveal the underlying reaction mechanism.

4. DECAY ANGULAR DISTRIBUTION

Since no new data has yet been reported, we use the older Aachen [4] data to illustrate the procedure, which yields the spin observables. The angular distribution $W(\theta,\phi)$ of the decay products of the vector meson is described in Ref. [4] for the cases of $\rho \to \pi\pi$ and $\phi \to \bar{K}K$ in terms of rest frame density matrix elements ρ_{ij} as

$$W(\theta,\phi) = \frac{3}{4\pi}[\frac{1-\rho_{00}}{2} + \frac{3\rho_{00}-1}{2}\cos^2\theta - \sqrt{2}\,\Re\ \rho_{10}\sin 2\theta\cos\phi - \rho_{1-1}\sin^2\theta\cos 2\phi]. \quad (3)$$

To express this angular distribution in the c.m. frame, it is convenient to describe W in terms of the angles $\bar{\theta},\bar{\phi}$ between the momentum of the produced vector meson and the velocity difference vector $\Delta\vec{v} = \vec{v}_1 - \vec{v}_2$. Here the velocities $\vec{v}_1$ and $\vec{v}_2$ represent the two velocities in the c.m. frame of the two decay mesons, respectively. With these new angles it is straightforward to obtain a new angular distribution $\bar{W}(\bar{\theta},\bar{\phi})$ in the c.m. frame,

$$\bar{W}(\bar{\theta},\bar{\phi}) = \frac{1}{(\sin^2\bar{\theta} + (\frac{E_\rho}{m_\rho})^2\cos^2\bar{\theta})^{3/2}} W(\theta(\bar{\theta}),\phi). \quad (4)$$

The angles θ and $\bar{\theta}$ are related by $\theta(\bar{\theta}) = \arctan(\frac{m_\rho}{E_\rho}\tan\bar{\theta})$, and $\phi = \bar{\phi}$.

In Ref. [4] where photon beam and nucleon target are unpolarized, the above angular distribution $\bar{W}(\bar{\theta},\bar{\phi})$ will depend only on the tensor polarizations T_{20}, T_{21}, T_{22} of the produced vector meson, but not on its vector polarization P_y [3]. The expression for $\bar{W}$ is

$$\bar{W}(\bar{\theta},\bar{\phi}) = \frac{1}{4\pi}\xi(\bar{\theta})[(1 - \sqrt{\frac{1}{2}}T_{20}(3\cos^2\bar{\theta}-1) + \sqrt{3}\ T_{21}\sin 2\bar{\theta}\cos\bar{\phi} - \sqrt{3}\ T_{22}\sin^2\bar{\theta}\cos 2\bar{\phi}],$$

where $\xi(\bar{\theta})$ is a simple kinematical factor. Once the angular distribution $\bar{W}(\bar{\theta},\bar{\phi})$ is determined, the appropriate projection produces the spin observables T_{20}, T_{21}, T_{22}.

5. CONSTRAINTS ON SPIN OBSERVABLES

In carrying out this procedure, we found that some results of the data analysis of Ref. [4] imply a negative $\bar{W}$ and had to be rejected. This fact makes it very clear that there are constraints on the allowed values of the vector meson's tensor polarizations T_{20}, T_{21}, T_{22}. These constraints have their origin in the physical requirement that the spin density matrix is positive definite [5,6]. This requirement leads to both linear and quadratic conditions on the spin observables T_{20}, T_{21}, T_{22}. It means that there are specific allowed domains for the values of the spin observables and that in any analysis those bounds should be respected. As an example, the bounds in the 2D subspace of T_{20} versus T_{21} are shown in Fig. 2.

6. CONCLUSION

These bounds also constrain the possible shapes of the decay distribution $\bar{W}(\bar{\theta}, \bar{\phi})$. An allowed shape of $\bar{W}$ with $T_{20} = -0.72, T_{21} = -0.21, T_{22} = 0.19$, is shown in Fig. 3.

In new experiments, the photon beam and possibly the nucleon target will be polarized, and therefore several new double spin observables will be measured. Again, limits on double spin observables can be obtained and these limits should be incorporated directly in the analysis.

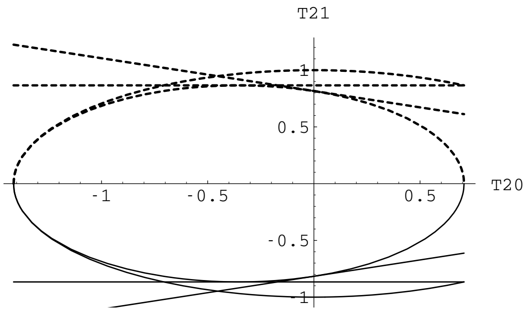

Figure 2. Domain in T_{21} versus T_{20} space is determined by combining upper bounds (dashed) and lower bounds (solid).

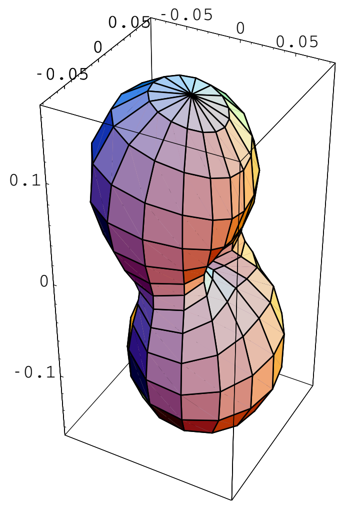

Figure 3. Shape angular distribution $\bar{W}$ for $T_{20} = -0.72, T_{21} = -0.21, T_{22} = 0.19$.

REFERENCES

1. M. Pichowsky, C. Savkli, and F. Tabakin , Phys.Rev. C53 (1996) 593.
2. K. Schilling, P. Seyboth and G. Wolf, Nucl. Phys. B15 (1970) 397.
3. W.M. Kloet, W-T. Chiang and F. Tabakin, Phys. Rev. C 58 (1998) 1086.
4. Aachen *et al.* Collaboration, Phys. Rev. 175 (1968) 1669.
5. P. Minnaert, Phys. Rev 151 (1966) 1306.
6. J. Daboul, Nucl. Phys. B4 (1968) 180.